THE EFFECT OF ANNEALING THIN FILM PARYLENE C-PLATINUM INTERFACES CHARACTERIZED BY BROADBAND DIELECTRIC SPECTROSCOPY

Eugene J. Yoon[1], Angela C. Stelson[2], Nathan D. Orloff[2], Christian J. Long[2], James C. Booth[2], and Ellis F. Meng[1]

[1]Department of Biomedical Engineering, University of Southern California, USA

[2]Radio Frequency Electronics Group, National Institute of Standards and Technology, USA

ABSTRACT

Thin film Parylene C has increasingly been employed as a substrate material with metals like platinum (Pt), especially in MEMS implantable devices. To assist in device design, broadband dielectric spectroscopy (up to 110 GHz) can characterize such materials with unique advantages unavailable in more-commonly used electrochemical impedance spectroscopy (up to 1 MHz).

In this work, coplanar waveguides (CPWs) fabricated from electron-beam evaporated Pt coated with Parylene C were measured with broadband dielectric spectroscopy to characterize the effect of thermal annealing. We confirmed that annealing caused no significant changes in Parylene C permittivity (2.85 ± 0.13 and 2.80 ± 0.18 before and after annealing; respectively) and extended the upper frequency limit to 110 GHz for the known permittivity value. Pt resistivity was unexpectedly reduced by 20% from annealing. Results and implications herein may inform fabrication-related design considerations of implantable devices using thin film Parylene C and Pt metal with radio frequency (RF) applications such as wireless power and data transfer.

KEYWORDS

Parylene C, Platinum, Thin film, Dielectric, Spectroscopy, Interfaces, Annealing, Thermoforming

INTRODUCTION

MEMS-based implantable devices featuring thin film polymer and metal interfaces have gained increased attention due to advantages such as biocompatibility, flexibility, cost, and softness [1]. Examples of commonly used polymers include polystyrene [2], liquid crystal polymer [3], SU-8 [4], polydimethylsiloxane [5], and Parylene C [6]. Of these, Parylene C, herein referred to as Parylene, is a popular choice by virtue of its amenability to micromachining techniques and its Class VI designation (the highest for medical plastics) from the U.S. Pharmacopeia [7].

Implantable devices can use RF techniques to wirelessly transfer data or power, which circumvents infection risks inherent in traditional percutaneous leads. Research on Parylene-based RF implantable devices is wide-ranging, encompassing intravascular blood pressure sensors [8], intraocular pressure sensors [9], implantable drug micropumps [10], and neurostimulators for activating muscles [11]. Parylene encapsulated coils have been even used in FDA-approved implantable devices such as the Argus II for wireless power transfer to retinal prosthetics, which partially restores vision to blind patients by electric stimulation of the retina [12].

Electrochemical impedance spectroscopy (EIS) has extensively characterized the reliability and integrity of Parylene-metal thin film interfaces [13], and RF dielectric spectroscopy may contribute to such studies. EIS is limited to approximately 1 MHz and the technique is performed in liquid electrolyte solution which can contribute to metal-polymer delamination. Dielectric spectroscopy can be performed both in wet or dry conditions and its broadband capabilities enable investigation towards wireless transfer loss mechanisms or microwave phenomena such as water dipole relaxation [14]. However, it is challenging to obtain extremely high frequency (EHF) measurements due to limited availability of EHF vector network analyzer (VNA) equipment.

RF investigation as a function of microfabrication post-processing techniques such as thermal annealing is additionally scarce. For instance, the influence of Parylene C on passive millimeter-wave circuits and a monolithic-microwave integrated circuit amplifier was studied up to 67 GHz [15], but only for as-deposited Parylene. In medical applications, Parylene is commonly annealed after deposition by heating it above its glass transition temperature but below its melting point in a vacuum environment. This increases polymer chain mobility to allow semi-crystalline and amorphous regions to reorganize and improve the film's crystallinity [16]. Such changes improve moisture barrier properties to benefit medical devices, but the molecular rearrangement may alter dielectric properties because the base molecule structure of Parylene C is polar [7] (Figure 1). For instance, other commonly used polymers such as SU-8 demonstrated non-negligible loss tangents at high frequencies (about 0.03 at 110 GHz) [17].

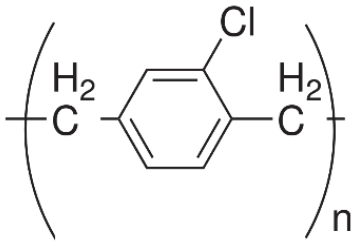

Figure 1. Base molecular structure of Parylene C is polar due to a chlorine atom covalently bonded to the aromatic ring

In this work, Pt CPWs coated with Parylene were fabricated and characterized via broadband dielectric spectroscopy with tools and techniques of the U.S. National Institute of Standards and Technology. We confirmed that annealing caused no significant changes in Parylene permittivity, but the Pt resistivity was reduced by 20%. These data can support the development of RF systems for implantable medical devices incorporating thin film polymers and metal.

MATERIALS AND METHODS

Microfabrication

Chips of dimension 1.1 cm × 1.1 cm (Figure 2) with CPW transmission lines of varying lengths (0.420 mm, 1.000 mm, 1.735 mm, 3.135 mm, 4.595 mm, 7.615 mm, and 9.970 mm), series resistors, series capacitors, and short-circuit reflects were fabricated on 500 µm thick, 100 mm diameter fused silica wafers. After spin coating and patterning AZ 5214-IR photoresist, a thin 8 nm layer of Pt with 1 nm of Ti as an adhesion layer was deposited via electron beam evaporation (FC/BJD-1800) to serve as a resistive element for series-resistor structures with 50 Ω nominal resistances.

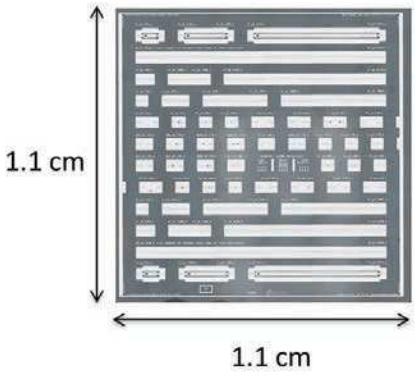

Figure 2. Optical micrograph of microfabricated chip with CPW structures such as lines, series resistors, series capacitors, and short-circuit reflects.

Following lift-off in acetone, isopropanol, and deionized water, another AZ 5214-IR layer was patterned and a thicker layer of Pt (200 nm) with 5 nm Ti was deposited to define the conductive structures. Afterwards, a total of 6.68 ± 0.03 µm (mean ± standard deviation) of Parylene C was deposited via conformal room temperature chemical vapor deposition (Labcoter 2 PDS 2010, Specialty Coating Systems). AZ P4620 photoresist was spun on and patterned to serve as an etch mask to protect against the following etch step in a deep reactive ion etcher (Oxford Plasmalab 100 ICP) [7]. On a subset of chips, all overlying Parylene was etched off. On others, the etch was limited to define contact pads for the VNA probes (Figure 3). Wafers were then diced (Disco DAD 3220) into chips. After the first set of measurements, the Parylene chip was annealed at 200 °C for 48 hours in a N_2 purged, vacuum oven (TVO-2 Cascade TEK).

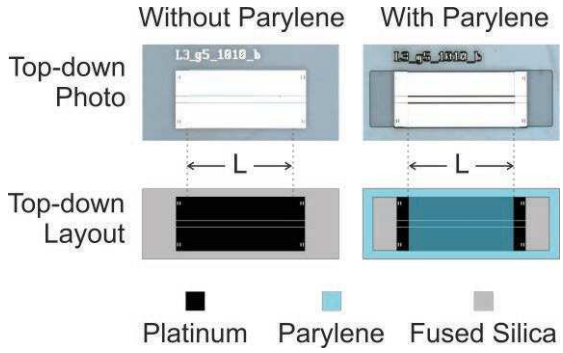

Figure 3. Micrographs and schematics illustrating a CPW transmission line with and without Parylene C.

Measurement and Simulations

On-chip S parameter measurements were acquired with a VNA (VectorStar MS4640A) and probes (GSG 100 i110-A) on a temperature-controlled stage at 37 °C (Figure 4). 617 frequency points from 40 kHz to 110 GHz were captured with AC power as -15 dBm (where 0 dBm was 1 milliwatt) with 10 Hz intermediate frequency bandwidth. Measurements were calibrated by a two-tier method modified from those of [14].

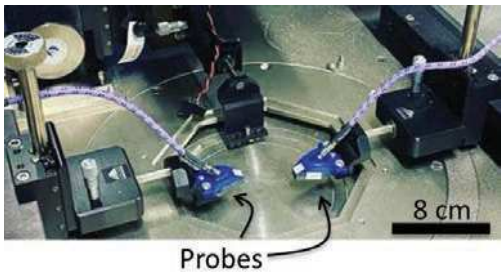

Figure 4. Photograph of temperature-controlled stage and probe tips which are connected to VNA measurement equipment. (no chip shown)

Briefly, the first tier entailed multiline thru-reflect-line (MTRL) [18] and series resistor [19] calibrations techniques on chips containing bare CPW reference structures without Parylene. This process accounted for the effects of the measurement system and probes and extracted the propagation constant of the bare CPW, (γ_0), where $\gamma_0 = \sqrt{(R_0 + i\omega L_0)(G_0 + i\omega C_0)}$. R_0, L_0, G_0, and C_0 are distributed circuit parameters of the bare transmission line. G_0 was assumed to be zero for the low-loss fused silica substrate. Then, C_0 was solved for by using R_0 and L_0 values which had been simulated via ANSYS Quasi-3D to the extracted propagation constant from MTRL.

In the second tier, MTRL was used to extract the propagation constant of unannealed Parylene (γ_U) such that $\gamma_U = \sqrt{(R_0 + i\omega L_0)(G_U + i\omega C_U)}$. R_0 and L_0 were obtained from the first tier and may be assumed to be identical between the CPW with unannealed Parylene and the CPW with no Parylene. C_U and G_U were computed from γ_U and γ_0 as described in [5] using $(\gamma_U^2) * i\omega C_0 = (\gamma_0^2) * (G_U + i\omega C_U)$. This allowed for the extraction of distributed circuit parameters from 100 MHz to 110 GHz. We also fitted corrected S-parameters of devices to a mismatched transmission line model to determine distributed circuit parameters from 40 kHz to 110 GHz [20]. These redundant processes allowed for cross-verification of measurements. Fitted results were plotted by averaging the data from CPW structures of multiple lengths with shaded error bars representing one standard deviation. Mean R and C values and corresponding pooled standard deviations were calculated across the frequencies and reported as mean ± standard deviation.

The unannealed Parylene chip was annealed and the measurement and calibration procedures were repeated on the same chip. Additional ANSYS simulations (Figure 5) generated functions to map distributed circuit parameters into permittivity values of the unannealed and annealed Parylene.

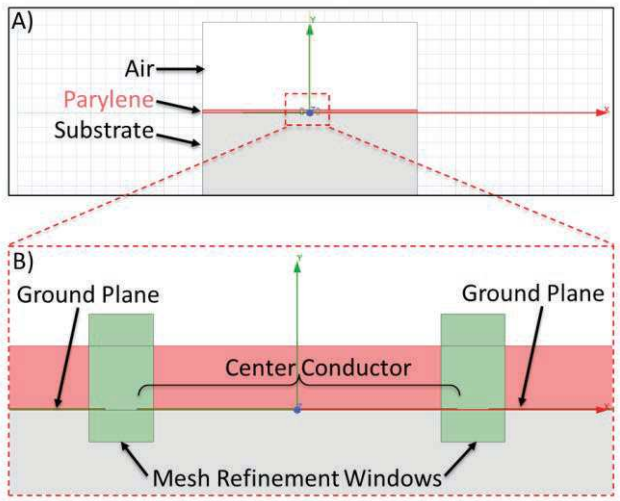

Figure 5. A) ANSYS Quasi-3D models simulated the Parylene coating on CPW cross sections. Inset B) Thin film Pt corresponding to the center conductor and two ground planes were beneath the Parylene and above the fused silica substrate. Mesh refinement windows were drawn at regions of interest to facilitate mapping function computation.

RESULTS AND DISCUSSION

The resistance per unit length of the same CPW chip before and after annealing was plotted (Figure 6). The high frequency rise in R is attributed to the skin effect and noteworthy data occur in the lower frequency plateaus (< 1 GHz) which may be extrapolated to DC resistance.

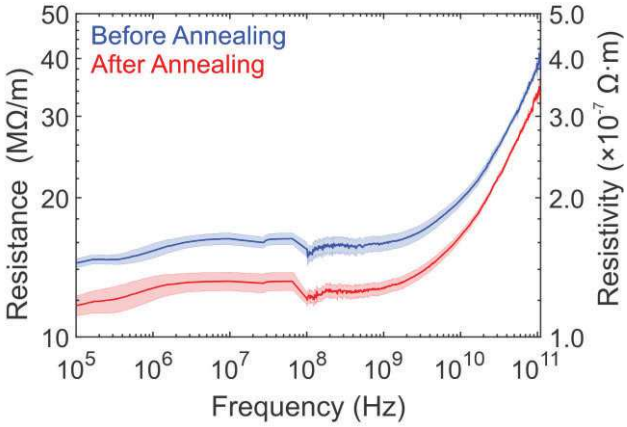

Figure 6. Resistance per unit length (left y-axis) and resistivity (right y-axis) of Pt before and after annealing.

A 20% decrease from 15.58 ± 0.55 MΩ/m to 12.53 ± 0.51 MΩ/m was measured before and after annealing from 1 GHz and below. The known geometry of the Pt layer allowed for computation of 155.8 ± 5.5 Ω·µm and 125.3 ± 5.1 Ω·µm resistivities. Bulk Pt resistivity is reported to be 106 Ω·µm and it is well-known that polycrystalline metal thin film resistivities are greater than that of their bulk material counterparts [21]. The decrease in resistivity from thermal annealing may be attributed to Pt approaching bulk property behavior due to relaxation of metal thin film stress and grain boundary reorganization.

Although these effects are known to occur for high temperature annealing (>400 °C) [22], the 200 °C process in this work yielded an unanticipated result which may inform future device design. For instance, many Parylene-Pt-Parylene devices with long aspect ratios are annealed after complete fabrication but have reported unwanted device curling [23]. Annealing before the second Parylene deposition may relax thin film stress such that less curvature is experienced. Additionally, lower film-to-film stress may potentially reduce rates of device delamination.

Simulated CPW modeling revealed that the majority of the electric field was concentrated inside the Parylene film and fused silica substrate (Figure 7).

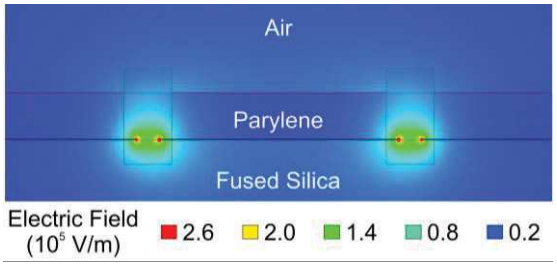

Figure 7. Modeling results demonstrated that the electric field is primarily confined within the Parylene film and fused silica substrate. This enabled the generation of a capacitance to permittivity mapping function

Based on simulations for the 6.68 µm Parylene thickness, a linear function mapping between capacitance to permittivity (ε) was generated where C (pF/m) = 12.15*ε + 96.949 (pF/m).

To within our uncertainty estimates, Parylene capacitance per unit length was approximately constant (Figure 8) as a function of frequency with no significant change before (131.62 ± 1.64 pF/m) and after annealing (130.91 ± 2.19 pF/m). The mapped corresponding ε values (2.85 ± 0.13 and 2.80 ± 0.18 before and after annealing; respectively) agreed well with previously reported values of 3.15, 3.10, and 2.95 at 60 Hz, 1 kHz, and 1 MHz; respectively [24]. This showed that molecular polymer chain rearrangement did not induce significant permittivity changes across a wide frequency range, indicating that Parylene C is well-suited for RF applications while extending the known permittivity to 110 GHz.

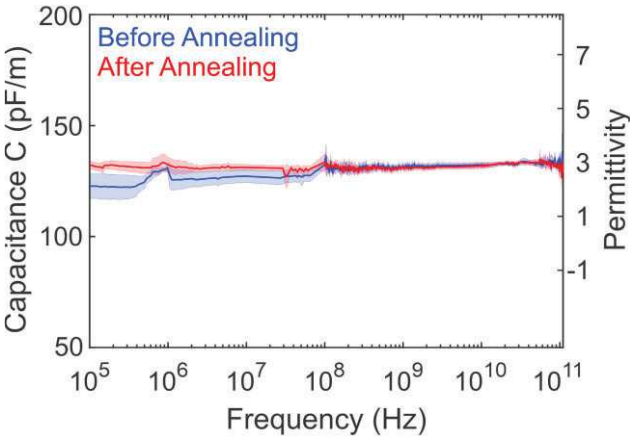

Figure 8. Capacitance per unit length (left y-axis) and permittivity (right y-axis) of Parylene before and after annealing.

CONCLUSION

In this work, coplanar waveguides were fabricated and coated with thin film Parylene to investigate material properties of the metal-polymer interface via broadband dielectric spectroscopy. We demonstrated that thermal annealing induced no change in Parylene permittivity but did cause an unexpected 20% reduction in Pt resistivity. These results may assist in future design of Parylene-based biomedical MEMS devices due to their implications on film stress and radio frequency loss factors. Future work will investigate RF circuit properties of Parylene-metal systems with respect to time spent soaking in saline solution.

ACKNOWLEDGEMENTS

This work was supported in part by the NSF under the INTERN supplement affiliated with Award IIP-1827773. The authors would like to thank Dr. K. Scholten for lending microfabrication expertise and the members of both the USC Biomedical Microsystems Laboratory and the NIST RF Team for their friendly support.

The content of the information does not necessarily reflect the position or the policy of the U.S. federal government, and no official endorsement should be inferred. Usage of commercial products and brand names herein is for information only; it does not imply recommendation or endorsement by NIST.

REFERENCES

[1] L. I. Bazylak, G. E. Zaikov, and A. K. Haghi, Polymers and Polymeric Composites: Properties, Optimization, and Applications. Apple Academic Press, 2014.

[2] K. Fukao and Y. Miyamoto, "Glass transitions and dynamics in thin polymer films: Dielectric relaxation of thin films of polystyrene," Phys. Rev. E - Stat. Physics, Plasmas, Fluids, Relat. Interdiscip., 2000.

[3] D. C. Thompson et al., "Characterization of liquid crystal polymer (LCP) material and transmission lines on LCP substrates from 30 to 110 GHz," IEEE Trans. Microw. Theory Tech., pp. 1343–1352, 2004.

[4] A. El Fellahi et al., "Microwave Sensor within a Microfluidic Chip for Biological Applications," Proceedings, vol. 1, no. 10, p. 523, 2017.

[5] S. J. Park, S. A. N. Yoon, and Y. H. Ahn, "Dielectric constant measurements of thin films and liquids using terahertz metamaterials," RSC, 2016.

[6] E. Yoon et al., "An implantable microelectrode array for chronic in vivo epiretinal stimulation of the rat retina," J. micromechanics microengineering, vol. 30, no. 12, 2020.

[7] J. Ortigoza-Diaz et al., "Techniques and Considerations in the Microfabrication of Parylene C Microelectromechanical Systems," Micromachines, p. 422, 2018.

[8] C. C. Yeh et al., "Fabrication of a flexible wireless pressure sensor for intravascular blood pressure monitoring," Microelectron. Eng., pp. 55–61, 2019.

[9] A. Shapero et al., "Wireless Implantable Intraocular Pressure Sensor with Parylene-Oil-Encapsulation and Forward-Angled RF Coil," 2019 IEEE 32nd MEMS Conf. pp. 21–24, 2019.

[10] A. Cobo, R. Sheybani, H. Tu, and E. Meng, "A wireless implantable micropump for chronic drug infusion against cancer," Sensors Actuators A. pp. 18–25, 2016.

[11] N. A. Sachs and G. E. Loeb, "Development of a BIONic muscle spindle for prosthetic proprioception.," IEEE Trans. Biomed. Eng., pp. 1031–1041, Jun. 2007.

[12] J. D. Weiland, S. Member, and M. S. Humayun, "Retinal Prosthesis," IEEE Trans. Biomed. Eng., pp. 1412–1424, 2014.

[13] R. Caldwell, M. G. Street, R. Sharma, P. Takmakov, B. Baker, and L. Rieth, "Characterization of Parylene-C degradation mechanisms: In vitro reactive accelerated aging model compared to multiyear in vivo implantation," Biomaterials, pp. 119731, 2020.

[14] C. A. E. Little, et al., "Modeling electrical double-layer effects for microfluidic impedance spectroscopy from 100 kHz to 110 GHz," LOC, pp. 2674, 2017.

[15] C. Kärnfelt et al., "Investigation of parylene-C on the performance of millimeter-wave circuits," IEEE Trans. Microw. Theory Tech., pp. 3417–3424, 2006.

[16] B. J. Kim, B. Chen, M. Gupta, and E. Meng, "Formation of three-dimensional Parylene C structures via thermoforming," J. Micromechanics Microengineering, 2014.

[17] S. Liu et al., "Hybrid characterization of nanolitre dielectric fluids in a single microfluidic channel up to 110 GHz" IEEE Trans. Microw. Theory Tech., pp. 5063–5073, 2017.

[18] D. C. DeGroot, J. A. Jargon, and R. B. Marks, "Multiline TRL revealed," 60th ARFTG Conf. 2002.

[19] N. D. Orloff et al., "A compact variable-temperature broadband series-resistor calibration," IEEE Trans. Microw. Theory Tech., pp. 188–195, 2011.

[20] N. D. Orloff et al., "How to extract distributed circuit parameters from the scattering parameters of a transmission line," Microwave Measurement Symposium (ARFTG), 2017, pp. 1–5.

[21] S. Dutta et al., "Thickness dependence of the resistivity of platinum-group metal thin films," J. Appl. Phys., pp. 25107, 2017.

[22] A. W. Groenland, "Degradation processes of platinum thin films on a silicon nitride surface." 2006.

[23] K. Scholten, C. E. Larson, H. Xu, D. Song, and E. Meng, "A 512-Channel Multi-Layer Polymer-Based Neural Probe Array," JMEMS, pp. 1054–1058, 2020.

[24] S. Horn, Parylene Dielectric Properties. June 5, 2015. Accessed on January 12, 2021 [Online] Available: https://blog.paryleneconformalcoating.com/parylene-dieletric-properties

CONTACT

*E. Meng, tel: +1-213-740-6952; ellis.meng@usc.edu